CONFERENCE PRE-PRINT

MODELING OF H-MODE EAST EDGE PLASMA WITH IMPURITY SEEDING BY SOLPS-ITER 3.2.0 ON WIDE GRID.

I.Yu. SENICHENKOV
Peter the Great Saint Petersburg Polytechnic university
Saint Petersburg, Russia
Email: I.Senichenkov@spbstu.ru

K.V. DOLGOVA
Peter the Great Saint Petersburg Polytechnic university
Saint Petersburg, Russia
Email: ksenmarial@mail.ru

N.V. SHTYRKHUNOV
Peter the Great Saint Petersburg Polytechnic university
Saint Petersburg, Russia
Email: shtirx@gmail.com

E.G. KAVEEVA
Peter the Great Saint Petersburg Polytechnic university
Saint Petersburg, Russia
Email: kaveeva_78@mail.ru

V.A. ROZHANSKY
Peter the Great Saint Petersburg Polytechnic university
Saint Petersburg, Russia
Email: rozhansky@mail.ru

R. DING [1]
Institute of Plasma Physics, Chinese Academy of Sciences
Hefei, China
Email: rding@ipp.ac.cn

G. XU
Institute of Plasma Physics, Chinese Academy of Sciences
Hefei, China
Email: guoliang.xu@ipp.ac.cn

H. SI
Institute of Plasma Physics, Chinese Academy of Sciences
Hefei, China
Email: hsi@ipp.ac.cn

J. GUO
Institute of Plasma Physics, Chinese Academy of Sciences
Hefei, China
Email: jguo@ipp.ac.cn

Q. LI
Institute of Plasma Physics, Chinese Academy of Sciences
Hefei, China
Email: qiushi.li@ipp.ac.cn

[1]Corresponding author

K. LI
Institute of Plasma Physics, Chinese Academy of Sciences
Hefei, China
Email: kdli@ipp.ac.cn

K. WU
Institute of Plasma Physics, Chinese Academy of Sciences
Hefei, China
Email: wukai@ipp.ac.cn

L. WANG
Institute of Plasma Physics, Chinese Academy of Sciences
Hefei, China
Email: lwang@ipp.ac.cn

J. LIU
Institute of Plasma Physics, Chinese Academy of Sciences
Hefei, China
Email: jianbinliu@ipp.ac.cn

L. MENG
Institute of Plasma Physics, Chinese Academy of Sciences
Hefei, China
Email: lingyi.meng@ipp.ac.cn

Abstract

In the paper the recently developed SOLPS-ITER 3.2.0 code is applied to model EAST H-mode impurity seeded shots with full account of drifts and currents, with kinetic treatment of neutrals (by the coupling to Monte-Carlo code Eirene) and on the fully unstructured grid extended up to real in-vessel structures. Thus the complexity of the physical model solved by SOLPS-ITER 3.2.0 on the extended grid reached the typical complexity level of models solved by SOLPS-ITER 3.0.8 on standard grids. The results obtained by SOLPS-ITER 3.2.0 are verified versus the corresponding SOLPS-ITER 3.0.8 cases and versus the experiment. For considered shots with Ne and Ar seeding it appears that a big amount of power should be radiated by the impurity in order to reproduce both the absorbed discharge power and outer target profiles. However, the radiated power and corresponding impurity concentration may be reduced if the radial energy flux towards the wall across the B-field increases – physically this corresponds to the convective energy flux towards the main limiter of the EAST machine. On the structured grid (SOLPS-ITER 3.0.8) this energy flux may be controlled by adjusting some parameters in boundary conditions applied on the virtual boundary representing a wall, while an account of toroidally non-symmetric limiter within the approach of an extended unstructured grid (SOLPS-ITER 3.2.0) appears to be not straightforward and might require further code development. In the DDN (disconnected double null) topology of EAST discharges the impurity tends to radiate not only from the bottom active divertor, but also from the vicinity of the top inactive X-point. The appearance of this secondary radiating spot is studied basing on the modeling results analysis.

1 INTRODUCTION

A long-time operation of future fusion tokamak-reactors requires a mitigation of particle and heat fluxes not only to divertor targets [1, 2] but also to other wall elements [3, 4]. The strength of these fluxes depends on the radial transport properties in the far SOL (Scrape-Off Layer), where the heat flux in electron channel already decays while the density is still big. To better understand these transport properties the 2D transport codes were significantly improved recently to operate on irregular (or unstructured) grids with boundaries coinciding to the real wall shape, so-called extended grids, see e.g. [5, 6, 7]. However, no successful results on modeling the edge plasma with full account of drifts and current on such grids were reported.

The SOLPS-ITER version 3.2.0 with a support of unstructured grids was launched several years ago [7]. However, only after couple of years a successful SOLPS-ITER 3.2.0 drift case was presented [8], but only on old structured grids. A converged drift case on unstructured grid was presented in [9], but still without a coupling to Eirene and without impurities.

In the paper the new code SOLPS-ITER 3.2.0 is for the first time successfully applied to model the plasma edge of EAST H-mode discharges with full drifts, impurities and kinetic neutrals. The brief description of the required

modification to SOLPS-ITER 3.2.0 may be found in [10]. The remaining restriction at present moment in SOLPS-ITER 3.2.0 is the absence of so-called 'void' regions of Eirene computational domain not covered by B2.5 mesh – this means that B2.5 and Eirene domains coincide. This restriction caused some difficulties in producing a plausible unstructured mesh to allow for an acceptable description in regions below the dome umbrella and in the shadow of the limiter, which is not toroidally symmetric. Two options for production of unstructured meshes are considered: a mesh extended into far SOL as if there is no limiter at all, and a toroidally symmetric limiter. For both cases it is demonstrated that solutions on structured and unstructured meshes (obtained by SOLPS-ITER 3.0.8 and 3.2.0 correspondingly) are very similar, excepting the zones where the computational domain is extended.

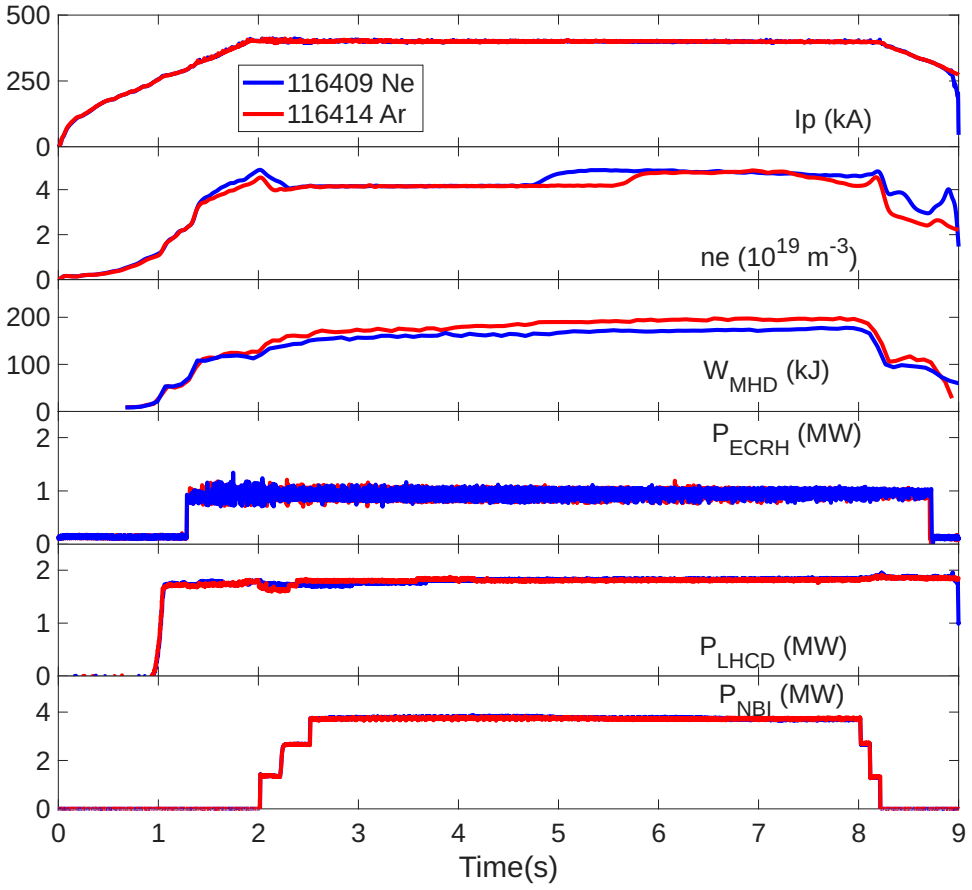

FIG. 1. Time traces of plasma current, line averaged electron density, MHD stored energy and auxiliary heating (ECRH, LH and NBI) power for EAST shots #116109 and #116114

With the second option (toroidally symmetric limiter) it is possible to achieve better coincidence to the experiments by choosing the boundary conditions (and their parameters on the limiter surface), which actually means the control of the power flux into the limiter shadow. On the mesh without a limiter there is no such a control, and a balance between the power entering the far SOL and the radiated power is shifted towards the increase of the impurity density and the radiation. The interesting feature of this solution is the presence of a radiating spot near the upper inactive X-point, so that the extra power which does not go into the limiter shadow is radiated from this spot. The appearance of such a spot looks typical for the experiments in the DDN magnetic topology [11, 12], and is also may be seen in modeling results, e.g. [13, 14].

2 MODELING SETUP

The time traces of two similar EAST discharges (#116409 with Ne seeding and #116414 with Ar seeding) are presented in Fig. 1. To perform a modeling with SOLPS-ITER, three meshes are produced, see Fig. 2: one standard mesh for 3.0.8 version and two unstructured meshes (without a limiter at all and with toroidally symmetric limiter) for 3.2.0 one, all in DDN topology stemming from the EAST equilibrium reconstruction. To account for the important neutrals flow beneath the dome from inner to outer divertor it is essential to include this region into the unstructured meshes, otherwise the computed inner divertor density is too big. The corresponding mesh 'us1' is therefore treated as non-satisfactory and is not shown here.

The fueling is applied via the SMBI from the outer midplane (OMP) with the rate $2.5 \cdot 10^{21}$ D atoms/s, the seeding is from the divertor in a form of mixture of equal number of impurity atoms and D2 molecules. The power entering the computational domain from the core is reduced to 3.0 MW thus effectively accounting for the core radiation. Since the corresponding radiating impurity species are not identified on EAST, they all are effectively represented by either Ar or Ne in the modeling. Only the steady-state modeling of a phase before the actual impurity seeding is considered in the paper ($t = 3.1s$ as in Fig. 1), modeling of other phases (including a dynamic

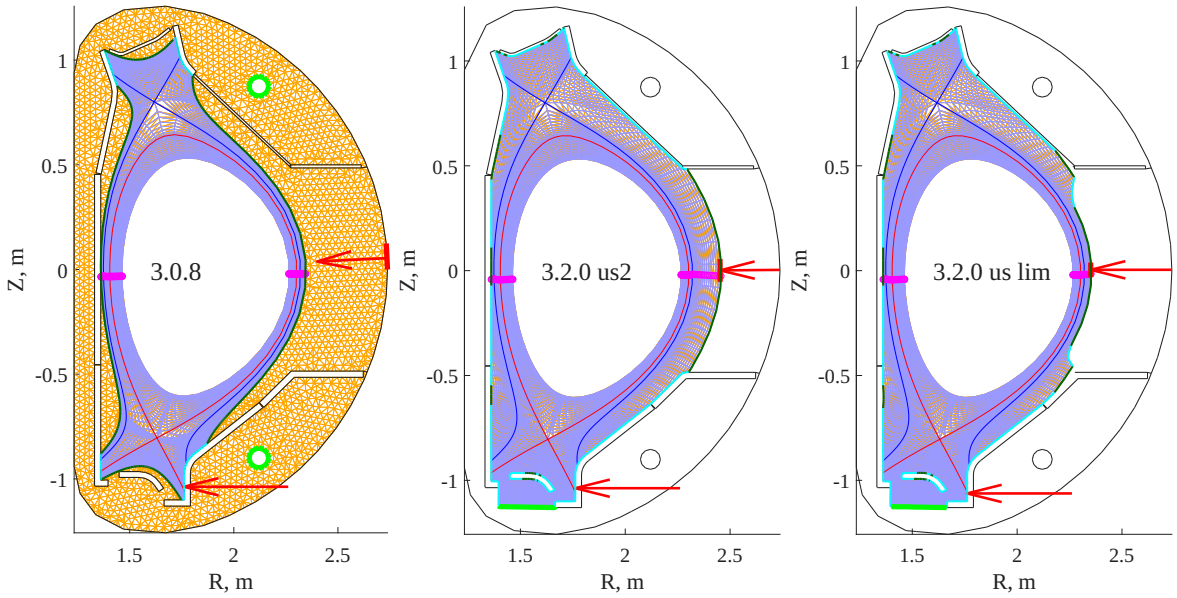

FIG. 2. Standard mesh for SOLPS-ITER 3.0.8 modeling and two unstructured (us) meshes for SOLPS-ITER 3.2.0 (without limiter and with toroidally symmetric limiter.)

transition between them) is left for the future.

The $D+$ ion flux (due to NBI) from the core side is set to $8 \cdot 10^{20}$ s^{-1}, the net impurity flux is zero. On the outer computational domain boundaries either 'sheath' or 'leakage' boundary conditions (BC) are applied, 'leakage' means that radial fluxes are set to be a small fraction of sound speed flux, like $\Gamma_{ir} = \alpha n_i c_s$. The choice between them is governed by the pitch angle between B-field and wall elements, see more details in [10] – boundary fragments are highlighted by color in Fig. 2. Formally, parameters α may be set separately for each boundary fragment, like e.g. artificial wall boundaries for standard mesh or limiter on unstructured mesh.

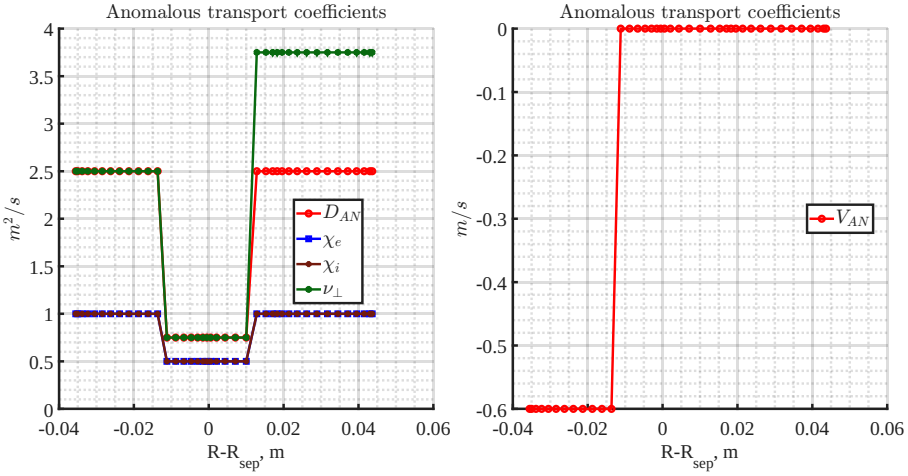

FIG. 3. Anomalous transport coefficeints used in SOLPS-ITER 3.0.8 to match experiments.

The seeding rate and the pumping efficiency (i.e. the fraction of neutral particles absorbed by pumping surfaces) are defined from requirements that the peak outer target (OT) T_e and the saturation current $j_{\parallel sat}$ match the experimental Langmuir probe data – the corresponding feedback loops are applied.

3 MODELING RESULTS.

3.1. Verification of SOLPS-ITER 3.2.0 versus 3.0.8 and the experiments

The first task is to fit the transport coefficients so that SOLPS-ITER 3.0.8 profiles match the experiments. These coefficients are shown in Fig. 3, while OMP and tagret profiles – in Figs. 4 and 5 with the label '3.0.8 to exp'.

An attempt to apply the same transport coefficients to SOLPS-ITER 3.2.0 on the mesh without the limiter ('us2' mesh) leads to the increase of the OMP density decay length and the increase of the impurity density, see profiles labeled as '3.2.0 us2' in Figs. 4, 5. The corresponding energy fluxes into the limiter shadow are smaller than in '3.0.8 to exp' cases, while the input power and power loads to the OT are the same (since target T_e and

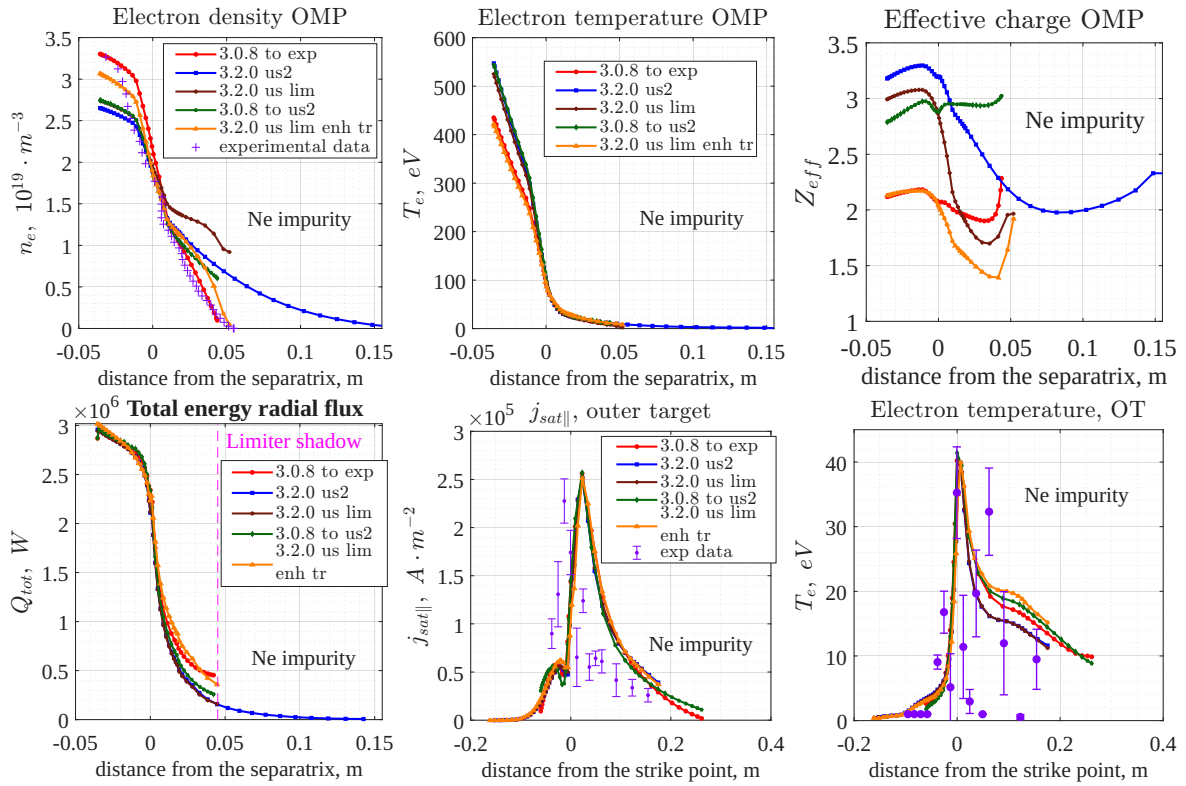

FIG. 4. OMP profiles of n_e, T_e, Z_{eff} and energy radial flux; OT profiles of $j_{sat\|}$ and T_e; Ne modeling cases.

$j_{\|sat}$ profiles are fitted). The rest of the power is radiated, and that's why the impurity density increases. Note that the radial density decay length on 'us2' mesh is defined by balance between radial and parallel transport and cannot be controlled by any input parameters, while on standard mesh (which ends before the entrance to the limiter shadow) it may be adjusted by α coefficients in leakage BCs applied on the virtual wall boundary.

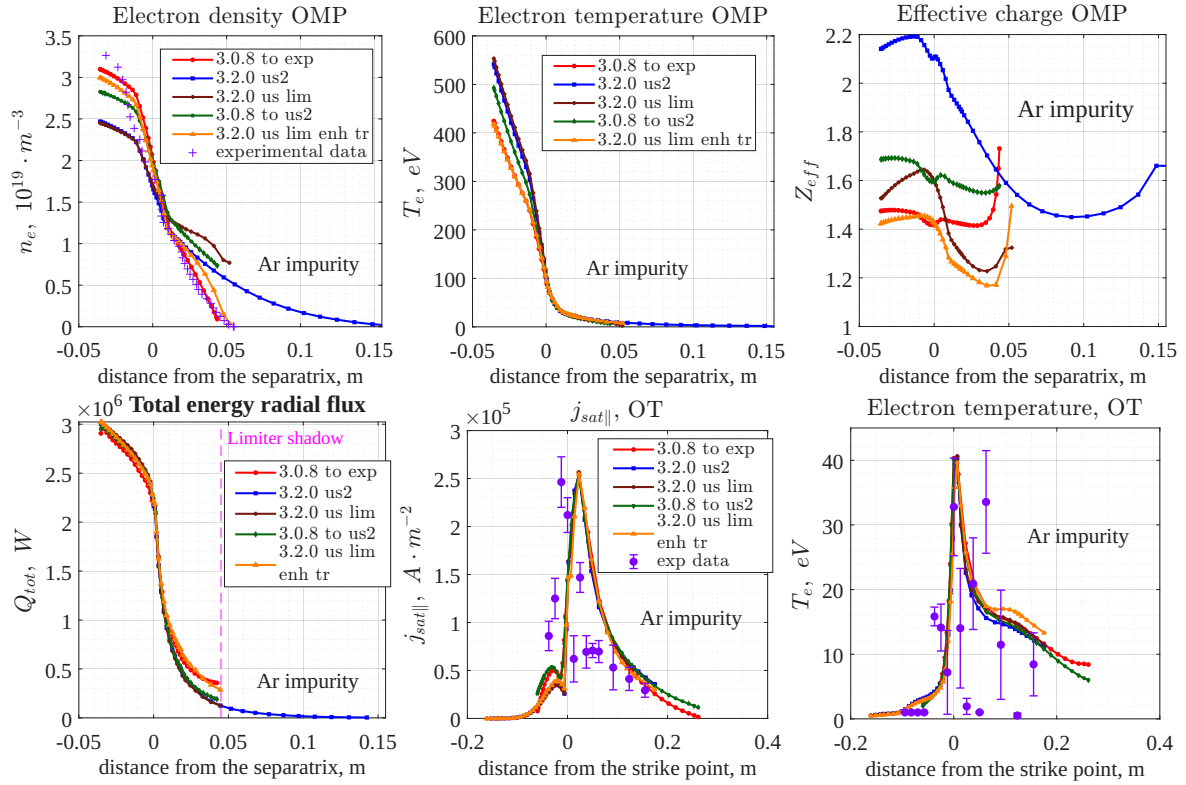

FIG. 5. OMP profiles of n_e, T_e, Z_{eff} and energy radial flux; OT profiles of $j_{sat\|}$ and T_e; Ar modeling cases.

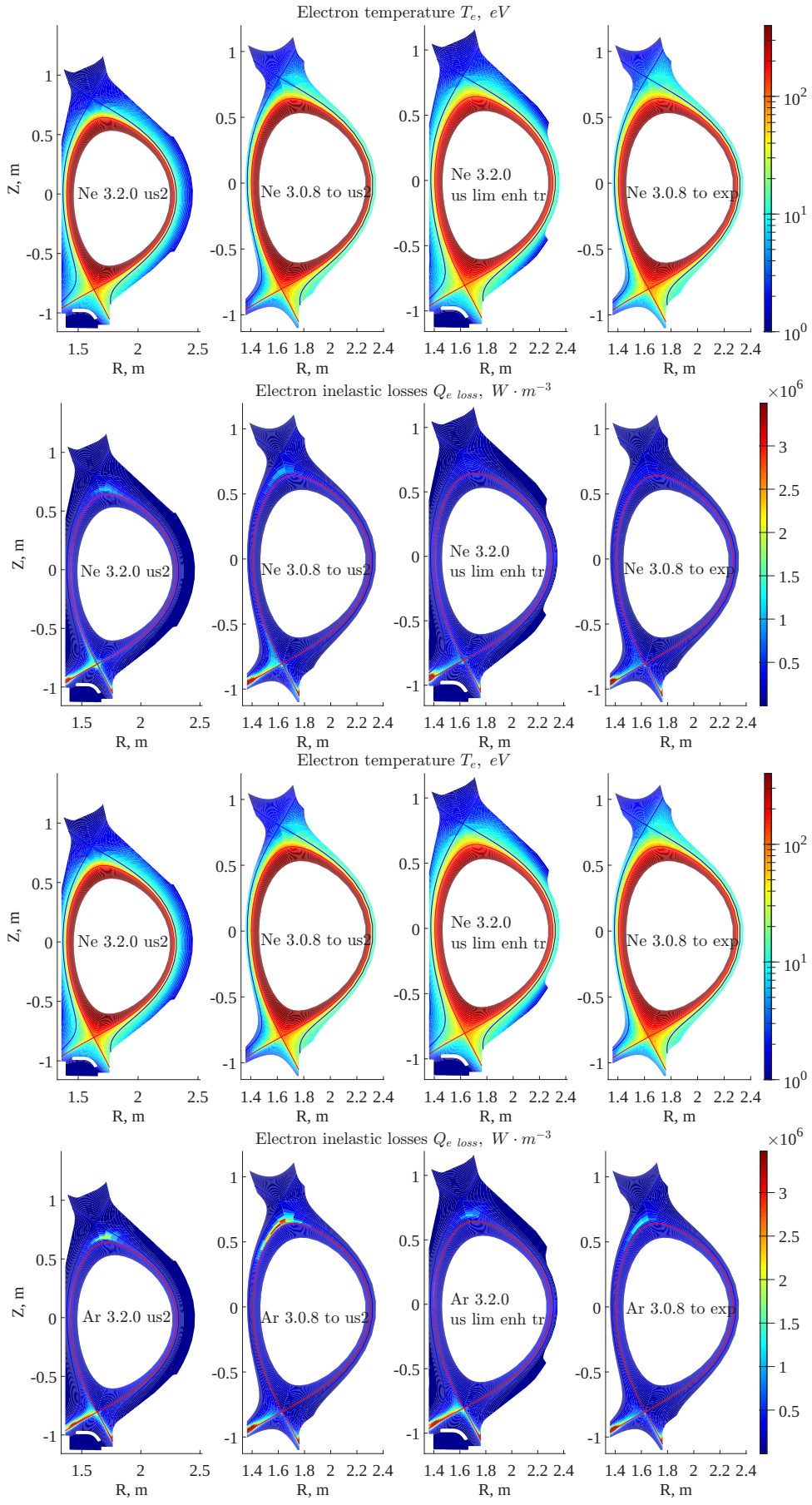

FIG. 6. 2D profiles of T_e and electron inelastic losses, which are approximately equal to radiation losses.

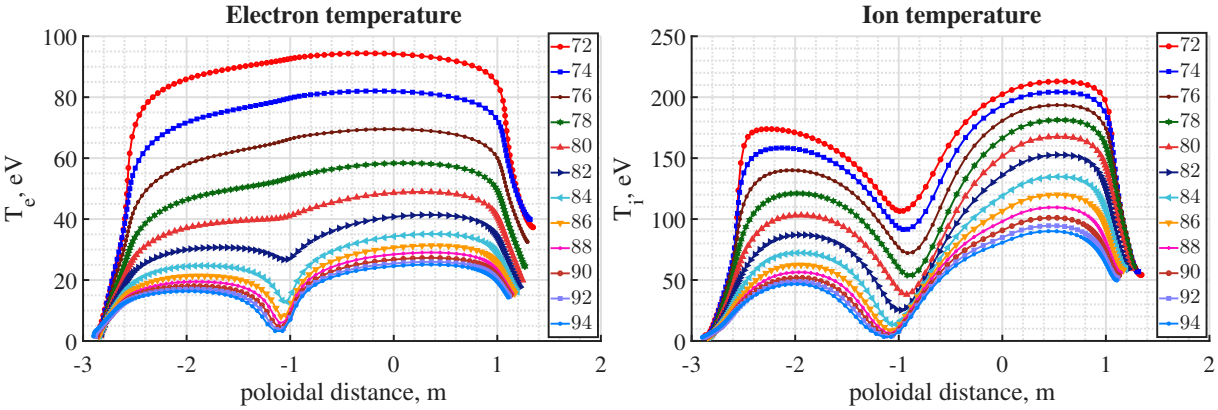

FIG. 7. Poloidal plots of T_e and T_i along flux tubes between primary and secondary separatrix from inner to outer lower targets, x=0 corresponds to OMP. Flux tube index increases from primary (72) to secondary (94) separatrix.

These α coefficents may be naturally adjusted so that SOLPS-ITER 3.0.8 profiles match SOLPS-ITER 3.2.0 profiles on 'us2' mesh rather than the experiments – this is the way how the case '3.0.8 to us2' is produced. By comparing these two cases it is possible to conclude that the SOLPS-ITER 3.0.8 and 3.2.0 code versions produce similar results for the same physical setup. Thus SOLPS-ITER 3.2.0 is verified vesrsus previous SOLPS versions.

To reproduce the experiments with SOLPS-ITER 3.2.0, in particular, the decay of n_e to zero near the limiter surface, it is necessary to introduce the limiter into the mesh. To address this task, the mesh 'us lim' is generated, where the limiter is assumed to be B-field aligned and toroidally symmetric. However, the simple run on the 'us lim' mesh doesn't lead to the reduction of density decay length and to the increase of the power into the limiter shadow. At least this power remains smaller than in '3.0.8 to exp' cases, because on standard meshes the whole virtual wall boundary works as the surface of energy sink, and its area is bigger than the actual limiter surface on 'us lim' mesh. In other words, the wall boundary of the standard mesh acts as toroidally symmetric limiter which is poloidally expanded from outer top to outer bottom target, and the energy sink on this limiter is controlled by α coefficients in the leakage boundary conditions.

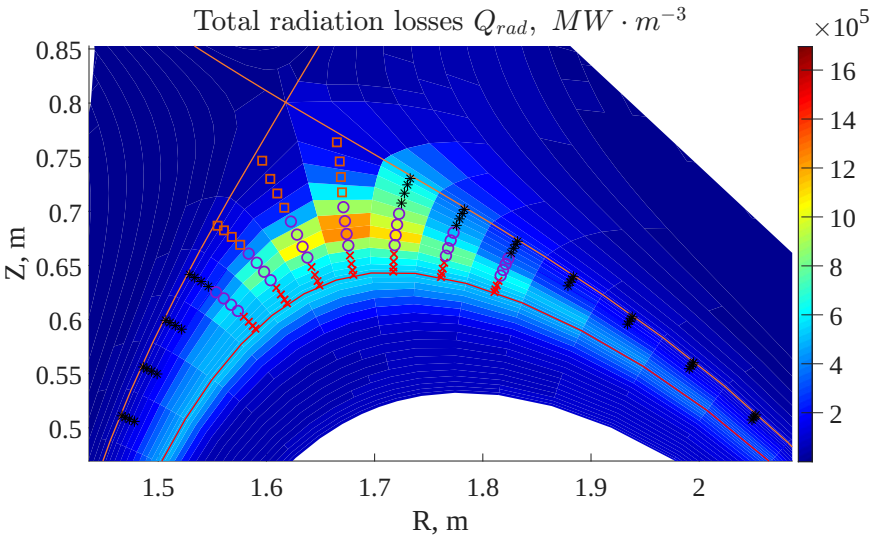

FIG. 8. Zones (group of cells on computational mesh) which are used for detailed energy balance analysis (plotted on the top of the 2D radiation losses). Red crosses represent the 4 innermost flux tubes; violet circles represent the 4 intermediate flux tubes; orange bars represent 4 outermost flux tubes; 'wings' on the 4 outermost flux tubes are marked via black asterixes.

So, to effectively increase the power into the limiter shadow in 3.2.0 modeling cases it is possible to apply the leakage boundary conditions on the limiter surface, and increase the α coefficients to force the density to decay to zero. Additionally, to transport the energy to the limiter surface, transport coefficient in the far SOL should be increased. The resulting profiles are shown as '3.2.0 to exp'.

3.2. Radiating spot below the upper X-point.

The 2D profiles of T_e and radiation losses are presented in Fig. 6. It may be noted that for cases with smaller energy flux into the limiter shadow ('3.2.0 us2' and '3.0.8 to us2') the radiation losses are bigger, and vice versa. The interesting feature of these cases is the appearance of the radiating spot below the inactive upper X-point, which here is very similar to the developed XPR near the active bottom X-point in dedicated experiments [15].

Poloidal profiles of T_e and T_i along all 12 flux tubes on the computational mesh in between primary and secondary separatrices for '3.2.0 us2' Ne case are shown in Fig. 7, and these flux tubes may be considered in groups with 4 tubes in each, Fig. 8. In the innermost zone the two main terms in the ion energy balance are the source via parallel heat conductivity and sink due to $B \times \nabla B$-drift convection, while no minimum in T_e is seen. For the 4 flux tubes in the middle, where the radiation losses are maximal, the main sink in the ion energy balance is the heat exchange with electrons. However, radiation losses are much bigger, and required energy is transported by the electron parallel heat conductivity. As a consequence, clear T_e minima are seen on these flux tubes. On the 4 outermost flux tubes all the energy flow along the flux tubes (both from the inner and outer midplane) is spent on the radiation in the 'wings' (also plotted in Fig. 8) before reaching the X-point, where the temperature falls down the level of 5 eV. Impurity neutrals penetrate inside the inactive separatrix from the top divertors, thus giving rise to the ionization source and impurity accumulation there. In spite of the relatively small losses on the neutrals ionization and on convective mixing (in the developed spot), they might be responsible for the initial T_i drop, as well as the the $B \times \nabla B$ convective cooling. This drop is enhanced due to the flux expansion if losses mentioned above are compensated by the parallel heat conductivity.

Investigation of the initial mechanism of the plasma cooling and impurity accumulation near the upper X-point is left for the future analysis. Nevertheless, due to mechanisms mentioned above the upper inactive X-point is favorable for the radiative spot formation.

4 CONCLUSIONS

In the paper SOLPS-ITER 3.2.0 modeling results of EAST Ar and Ne seeded H-mode disharges with account of full drifts and kinetic neutrals on fully unstructured mesh extended up to the wall are presented. A satisfactory agreement to the experiments and to older SOLPS-ITER version 3.0.8 (on structured mesh with the artificial wall boundary) is demonstrated. To achieve this agreement it is necessary to effectively increase the energy flux onto the surface of toroidally non-symmetric EAST main limiter, or into its shadow. Even in these cases the impurity content in the computational domain is big, its corresponding separatrix concentrations are $c_{sep}^{\mathrm{Ne}} \approx 1.8\%$, $c_{sep}^{\mathrm{Ar}} \approx 0.5\%$. In contrast, if the limiter is ignored (i.e. the unstructured mesh is toroidally symmetrically extended into the far SOL but without a limiter), the lack of the power escaping towards far SOL should be compensated by extra impurity radiation. In such modeling cases indeed the impurity concentration increases, and this extra power is radiated from a spot below the inactive upper X-point. The indications of the existence of such a radiating spot are found in ASDEX Upgrade and EAST DDN experiments as well as in the SOLPS-ITER modeling of other machines again in DDN topology. Since this spot is located in the SOL away from the confined region and the radiation from it reduces the heat loads to active targets, the investigation of physics, stability and control of regimes with this upper radiating spot is of interest. This task, however, is left for the future.

ACKNOWLEDGEMENTS

This work was supported jointly by the Russian Scientific Foundation (Grant No. 23-42-00020), National Natural Science Foundation of China (Grants 12261131496 and 12425509) and the CAS President's International Fellowship Initiative (PIFI). Numerical calculations were performed at the Polytechnic Super Computer Center at Peter the Great St. Petersburg Polytechnic University.

REFERENCES

[1] R.A. Pitts et al. *Nuclear Materials and Energy*, **20**, 100696, 2019.
[2] H. Reimerdes et al. *Nuclear Fusion*, **60** (6), 066030, 2020.
[3] R.A. Pitts et al. *Nuclear Materials and Energy*, **42**, 101854, 2025.
[4] F. Maviglia et al. *Nuclear Materials and Energy*, **26**, 100897, 2021.
[5] N. Rivals et al. *Nuclear Fusion*, **65** (2), 026038, 2025.
[6] W. Zhang et al. *Nuclear Fusion*, **63** (3), 036008, 2023.
[7] W. Dekeyser et al. *Nuclear Materials and Energy*, **27**, 100999, 2021.
[8] Ilya Senichenkov et al. *Contributions to Plasma Physics*, **64** (7-8), e202300136, 2024.
[9] N.V. Shtyrkhunov et al. *Technical Physics Letter*, **51**, 6–8, 2025.
[10] N. Shtyrkhunov et al. *IAEA FEC2025, TH/5-1, submitted to Nuclear Fusion*, **65**, 2025.
[11] A Redl et al. *Plasma Physics and Controlled Fusion*, **65** (11), 115003, 2023.
[12] Baoguo Wang et al. *Nuclear Fusion*, **65** (8), 086004, 2025.
[13] I.Yu. Senichenkov et al. *Nuclear Fusion*, **62** (9), 096010, 2022.
[14] Vladimir Rozhansky et al. *submitted to Contributions to Plasma Physics*, **66**, 2026.
[15] M. Bernert et al. *Nuclear Materials and Energy*, **43**, 101916, 2025.